MDPI

*Article*

# Hybrid Ceramic Self-Healing Coatings for Corrosion Protection of Al Alloys in 3% NaCl Solution

**Stefano Mori [1],\*, Francesca Romana Lamastra [2] and Giampiero Montesperelli [2]**

1    Energy and Sustainability Theme, Cranfield University, College Road, Cranfield MK43 0AL, UK
2    Dipartimento di Ingegneria dell'Impresa "Mario Lucertini" and Consorzio INSTM Unità di Ricerca "Roma Tor Vergata", Università degli Studi di Roma "Tor Vergata", Via del Politecnico, 00133 Roma, Italy; lamastra@scienze.uniroma2.it (F.R.L.); montespe@stc.uniroma2.it (G.M.)
\*    Correspondence: stefano.mori@cranfield.ac.uk

**Abstract:** This work focuses on the development of sol–gel self-healing coatings for corrosion protection of Al alloys. The use of this method will help to reduce the costs associated with the coating as well as their environmental impact. Coatings were made of a titania matrix loaded with microparticles of poly(vinyl-alcohol) (PVA) containing cerium nitrate as an inhibitor. The PVA particles dissolve in water, so that the cerium nitrate deposits on the Al surface subjected to corrosion. The PVA microspheres were made via the emulsion method, and then loaded with cerium nitrate. The amount of cerium nitrate loaded in the microspheres was evaluated using UV–Vis. As a second step, the titania coating with embedded PVA microspheres loaded with cerium nitrate was deposited on an AA6082 substrate via a sol–gel route. The corrosion resistance of the coated samples was tested in NaCl solution. The coating microstructure, before and after the corrosion tests, was analysed with the use of an SEM (scanning electron microscope) and EDS (energy dispersive spectroscopy), while the corrosion resistance was investigated by EIS (electrochemical impedance spectroscopy). The results showed that the coatings were uniform and compact. They also showed the ability of the hybrid TiO$_2$-based coating to provide protection for the AA6082 from corrosion. The coatings with an induced defect (scratch) were also analysed, and the EIS analysis of the coatings over time showed an increase in resistance, confirming the ability of the coating to heal itself.

**Keywords:** corrosion; coating; self-healing

## 1. Introduction

Since the discovery of chromium (VI) toxicity [1], there has been an opening for replacing its use in coatings for corrosion protection. Over the years, many researchers have been working on different coatings and coatings' techniques [2,3]. From phosphate or cerium-based conversion coatings [4,5], hybrid sol–gel organic–inorganic coatings [6–9], to physical vapour deposition (PVD) aluminium-doped zinc oxide films [10–12], high velocity oxygen fuel (HVOF) titania sprayed coating [13], sol–gel SiO$_2$, and ZrO$_2$ [14,15] have been extensively investigated as alternatives for chromate-base conversion coatings. More recently, attempts to develop self-healing coatings have been made to protect Al alloys from corrosion [16–19]. Most of these coatings rely on high-temperature production routes and/or an ultra-high vacuum (UHV) such as PVD, chemical vapour deposition, and HVOF. This makes the manufacturing of these coatings costly and time consuming. Furthermore, most of the self-healing coatings are based on the incorporation of a corrosion inhibitor, which could be damaged by the application of high temperatures required by UHV techniques.

For this reason, the sol–gel route in depositing coatings has gained interest [9,14,20–24] over the years. This is due to a variety of reasons, which are linked to the temperature used during the process and low environmental impact of the reactant used in the process [9]. The sol–gel process has the benefit of reducing the costs incurred during the

coating procedure [25,26]. The quality of the final coatings relies on the control of several parameters, such as precursor selection, nature of the catalyst, duration of the process, and temperature [27,28].

Among the coatings' chemical composition tested, titania has shown excellent anticorrosion properties, due to its chemical stability, heat resistance, and low electron conductivity. Despite these, sol–gel-derived coatings were scarcely investigated [9,29–31]. Liu et al. prepared nano-$TiO_2$ coatings on an anodized aluminium surface by a vacuum dip-coating method and reported the excellent anticorrosion properties of the coating in sterile seawater at room temperature [7]. Poznyak et al. reported good anticorrosive protection of an AA2024 alloy in chloride solution provided by titania-based hybrid sol–gel coatings [32].

Many efforts have been focused on the realization of a new generation of coatings, called "smart" coatings. These coatings would have additional features such as a self-healing ability, which can be achieved with different designs. By self-healing, the coating is intended to have the ability to repair itself. One possible way to provide a self-healing ability to the coatings is to design a hybrid coating, i.e., the use of two (or more) different types of materials. One of the materials will act as a matrix and have a barrier effect, while the second will function as an inhibitor reservoir in case of damage to the matrix. In 2012, Zand et al. [33] reported the use of a self-healing coating on stainless steel 304. As stated in the article, the treatment of the metal surface with 3-glicidoxypropyltrimethoxy silane solution modified with cerium nitrate shows the formation of a transparent coating on the surface. The coating was prepared by the sol–gel technique and was able to protect the substrate from the corrosion and furthermore showed a self-healing ability.

The inhibition properties of cerium ions were widely discussed in the literature and several authors reported tests on the self-healing ability of the cerium-containing molecules [24,34,35]. Pepe et al. [20,35] reported that the incorporation of cerium ions in hybrid silica sol–gel coatings prepared by tetraethylorthosilicate [$Si(OC_2H_5)_4$, TEOS] and methyltriethoxysilane [$SiCH_3(OC_2H_5)_3$, MTES] doped with cerium salts on AISI 304 stainless steel and aluminium substrates resulted in an improvement in the corrosion protection. This is due to cerium (III and IV) for Al alloys and chromium (in the case of stainless steel) ions that reacted with the hydroxyl groups and caused the precipitation of cerium and chromium oxide/hydroxide on cathodic areas. These oxides (or hydroxides) can act as a barrier for a further oxygen reaction. Furthermore, Schem et al. [36] studied the behaviour of AA2024-T3 coated with a hybrid sol–gel containing nanoparticles of cerium oxide. They reported that the incorporation of ceria nanoparticles had a beneficial effect on corrosion performances. It was also demonstrated that the effect was dependent on the nanoparticle content. Montemor et al. [37] investigated the role of $CeO_2$ nanoparticles used as fillers for hybrid silane coatings applied on galvanized steel substrates. The studies were conducted by electro-chemical impedance spectroscopy (EIS) and scanning vibrating electrode technique (SVET). The measurements showed that the modified coatings had improved the barrier properties and increased the corrosion inhibition effect of ceria nanoparticles activated with Ce (III) ions.

Other articles can be found in the literature, for example, in 2007 Yabuki et al. [38] developed an organic coating and metal powder mixture for the corrosion protection of AA3003. Several formulations were tried, changing compositions, recipes, and curing temperatures. All the coatings had a final thickness of about 30 μm. They reported that every kind of coating offered a good protection against corrosion phenomena and these results were improved with the addition of a metal powder in the mixture.

Lamaka et al. [39] tried a different approach to the resolution of the self-healing problem. They coated the surface of an AA2024-T6 alloy with a porous titania layer. This layer acted as reservoir of inhibitor. After that, the samples were coated via the sol–gel technique. The addition of the reservoir resulted in an improvement in the anti-corrosive properties of the system and the aid of the inhibitor allowed the coating to repair itself once damaged.

Nesterova [40,41] developed a coating composed of a matrix made of epoxy resin with microcapsules based on poly(urea-formaldehyde). The microcapsules were filled with an inhibitor and then dispersed in the matrix. The paper concluded that such a system was able to retard the starting of the corrosion and then repair the damages on the surface of the coatings. Most of the works published made use of polymers as carrier of the inhibitor agent, but most of the reported polymers are not soluble in water, so they would require some other agent to trigger the self-healing property.

This work presents a new concept. The inhibitor agent (cerium nitrate) will be encapsulated in poly(vinyl-alcohol) (PVA), a polymer that is able to be dissolved in water and release the inhibitor. The coating matrix will be developed using green reagents and a low temperature (100 °C), which would be suitable for the use of PVA (melting temperature of about 120 °C) and deposited on an Al substrate. The PVA has been chosen for its solubility in water while cerium nitrate was chosen for its healing properties in Cl-containing environments.

## 2. Materials and Methods

### 2.1. Materials

2.1.1. Poly(vinyl alcohol) (PVA) Spheres Preparation

PVA (2 g) (Sigma-Aldrich, Milan, Italy, Mw = 13,000, CAS n° 9002-89-5) was dissolved in 40 mL of distilled water. The obtained solution was added to a continuously stirred solution of 20 mL of olive oil and 0.1 mL of Span80 (Sigma-Aldrich, CAS n° 1338-43-8), in the ratio 1:20. Then, the resulting emulsion was ultra-sonicated (Sonics, Newton, MA, USA, VibraCell VC 750, max power 750 W) for 3 min with an impulsive signal (3 s on, 3 s off) at 40% power. After that, the emulsion was heated at 80 °C for complete water evaporation. The resulted suspension was finally filtered with Sartorius PTFE filter (pore size 0.2 μm). The collected powder was dried at room temperature for a night.

2.1.2. Inhibitor Encapsulation

A calibration line was obtained using five solutions of cerium nitrate in de-ionised water at known concentrations (from $1.05 \times 10^5$ to $3.16 \times 10^{-5}$ M). The absorbance of the five solutions at known concentrations was used to build a calibration line, according to Beer–Lambert's law. The slope of the Beer–Lambert equation was then calculated.

A total of 1 mg of spheres was suspended in 1 mL of cerium nitrate ($Ce(NO_3)_3 \cdot 6H_2O$, Sigma-Aldrich, CAS n° 10294-41-4) solution in ethyl alcohol (10 g/L). The resulting mixture was left under agitation at room temperature and then filtered after different immersion times (0, 15, 30, 45, 60, 90, and 120 min). To measure the amount of Ce encapsulated after the different immersion times, a small amount of the mixture (50 μL) was collected, and then the solvent was left to evaporate. The dried residues were then dissolved in 50 mL of water and analysed by UV–Vis. The concentrations of cerium nitrate left in the suspension were calculated using the slope from the calibration line. Solutions were analysed using a UV–Vis spectrophotometer (UV–Vis Spectrophotometer UV-2450, Shimadzu, Milan, Italy) in the wavelength range 200–400 nm.

2.1.3. Substrate and Coatings Preparation

The substrate material used for the investigation was AA6082 with a chemical composition given in Table 1.

**Table 1.** Composition of aluminium alloy 6082 (wt%) [9].

| Al | Si | Fe | Cu | Mn | Mg | Zn | Ti | Cr |
|------|---------|-----|-----|---------|---------|-----|------|------|
| Bal. | 0.7–1.3 | 0.5 | 0.1 | 0.4–1.0 | 0.6–1.2 | 0.2 | 0.25 | 0.25 |

The samples with a size of $10 \times 20$ mm$^2$ and 1 mm thickness were polished up to 1000 grit. The preparation of the substrates is reported elsewhere [9]. TiO$_2$ coatings were prepared following the steps reported below:

1.     Dissolution of 3 mL of titanium tetra-isopropoxide (Sigma-Aldrich, CAS n° 546-68-9) in 50 mL of ethanol and 3 mL of acetic acid (with both functions of acid catalyst and chelating agent) under stirring at 200 rpm for 2 h, 30 mg of spheres with inhibitor were added.
2.     Immersion of the substrate in the solution for 30 s.
3.     Formation of a wet layer by extraction of the substrate at a speed of 4 cm/min.
4.     Gelation of the layer by solvent evaporation at room temperature for a night and subsequent destabilization of the sol.

To achieve a compact film, the samples were consolidated in a furnace at 100 °C with a slow heating rate (3 °C/min) to ensure a further poly-condensation of the colloidal particles entrapped in the liquid phase of the gel. A second solution without spheres was prepared and the procedure was repeated for a second time for the samples with two layers of coating. Samples with two TiO$_2$ layers without spheres were also prepared. A list of prepared samples, with labels, is given in Table 2. A schematic representation of the process is shown in Figure 1, while a schematic of the samples is shown in Figure 2.

**Table 2.** List of prepared samples.

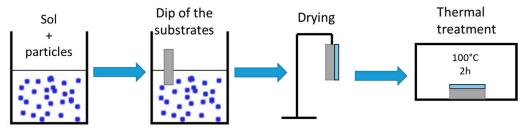| Sample | Dips with Spheres | Dips without Spheres |
|--------|:-----------------:|:--------------------:|
| Ti1DS | 1 | 0 |
| Ti1DS1DT | 1 | 1 |



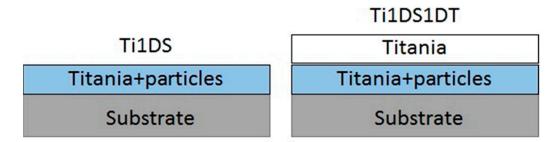**Figure 1.** Schematic diagram of the coating preparation.



**Figure 2.** The figure shows a schematic diagram of the samples prepared.

*2.2. Methods*

2.2.1. Coatings Characterization

The size distribution of the spheres was evaluated using an open-source image software (ImageJ) [42]. The microstructure of the coated samples was investigated with field emission scanning electron microscopy (SEM) (Zeiss, LEO Supra 35, Cambridge, UK) coupled with energy dispersive spectroscopy (EDS) (INCA X-sight, Oxford instruments, Oxford, UK).

X-ray photoelectron spectroscopy (XPS) was performed. The spectra were collected using an ESCALAB 250Xi (Thermo Fisher Scientific Ltd., Loughborough, UK) spectrometer,

equipped with a monochromatic Al Kα excitation source, electromagnetic lens system, 6-channeltron detector, and charge neutralisation by two flood sources: an in-lens filament for coaxial electron flux and a very low energy Ar+ ion gun. The measurements were carried out in standard electromagnetic mode (diameter of analysed area about 1 mm) at the pass energy of 20 eV. The binding energy (BE) scale was calibrated by setting the C1s peak of adventitious carbon (surface contamination) to BE = 285.0 eV. The spectroscopic data were processed by the Avantage v.5 software (Thermo Fisher Scientific Ltd., Loughborough, UK).

2.2.2. Electrochemical Characterization

EIS was performed in 3 wt% NaCl aqueous solution at room temperature (approximately 25 °C) for 7 days, by using a Solartron (Leicester, UK) SI 1287 Electrochemical Interface and a Solartron 1260 Frequency Response Analyser. The frequency ranged from $10^{-2}$ to $10^{5}$ Hz, imposing an alternating signal of 10 mV around the Open Circuit Potential (OCP). A platinum plate and an Ag/AgCl electrode were used as counter and reference electrodes, respectively. EIS spectra were acquired using Zplot and then analysed using Zview v4.0 software (Scribner Associates). Different equivalent circuits were used for the analysis. The non-linear least squares (NLLS) method and chi-squared test ($\chi^{2}$) were used to evaluate the goodness of the fit. Bare substrate was also tested.

To understand the self-healing ability of the coatings, the corrosion test was performed on samples with a scratched coating. The equivalent circuit used for the EIS analysis is shown in Figure 3. The equivalent circuit is composed of three resistances and two constant phase elements. The first resistance ($R_{sol}$) represents the resistance of the solution, the second one ($R_{pore}$) represents the resistance of the coating defects, while the last one ($R_{ct}$) represents the charge transfer resistance. The two constant phase elements represent the capacitance of the coating ($CPE_{coat}$) and the double layer capacitance ($CPE_{dl}$).
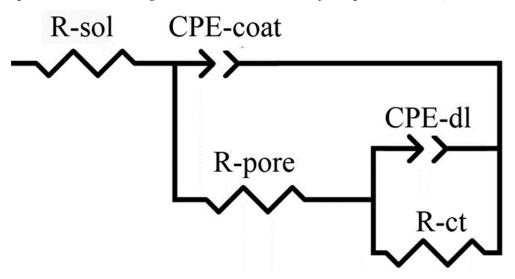


**Figure 3.** Equivalent circuit used for EIS fitting.

### 3. Results

*3.1. Microspheres Characterization*

The PVA particles obtained via the emulsion process were characterized morphologically. An SEM image taken after the drying process is shown in Figure 4. A distribution of diameters was obtained from the image and the size distribution analysis is reported in Figure 5. The distribution of the microspheres' diameters seems to peak between 200 and 400 nm. About 70% of the total spheres are around 200 and 600 nm, with a mean of the distribution of 500 nm. Only a small fraction (about 9%) is greater than 1 μm.
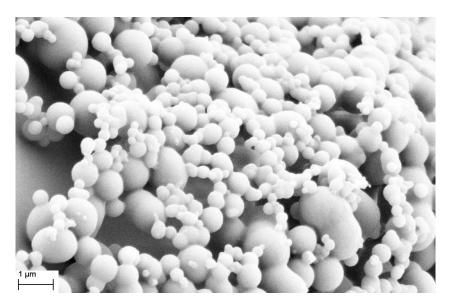
**Figure 4.** SEM micrograph (at 30 kx) of PVA microspheres.
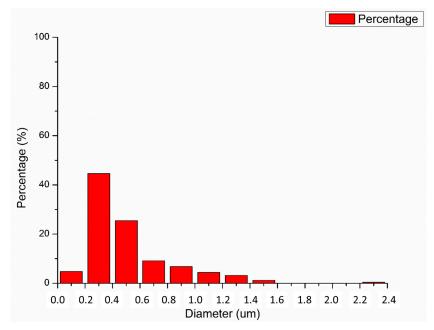


**Figure 5.** Size distribution of the spheres.

The spheres were then loaded with the corrosion inhibitor, using an impregnation technique. The system was calibrated using the Beer–Lambert law, $A = \varepsilon bC$, where $A$ is the absorbance, $\varepsilon$ is the molar attenuation coefficient, $b$ is the path length, and $C$ is the concentration. Five solutions of cerium nitrate were prepared at a known concentration as reported in Table 3. The peaks of absorbance were then plotted against the concentration, to obtain a calibration curve for the cerium nitrate (Figure 6). The slope calculated from Figure 6 is 24,479 $M^{-1}$.
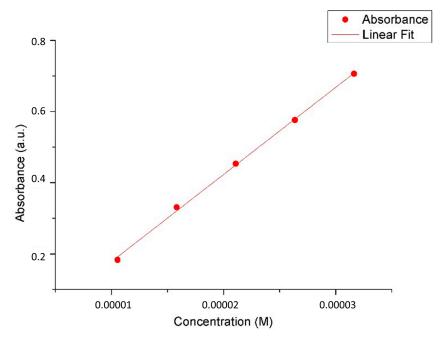
The spheres were dipped for different times into the alcoholic solution of inhibitor and the cerium nitrate concentration was evaluated by UV–Vis spectroscopy. Five different immersion time were investigated. A selection of spectra is shown in Figure 7. From the peak of the absorbance, the concentrations were calculated using the Beer–Lambert law, and then the difference between the initial concentration ($C_0$) and concentration after the immersion times ($C_t$) was attributed to the encapsulation and the adsorption process. Considering the mass (in mg) of adsorbed molecules per mg of sphere in the solution (Figure 7), it can be seen that the maximum of the encapsulation is obtained at 90 min for

this system. The amount of cerium nitrate contained was about 1.5 mg per mg of spheres. The coatings were prepared using the spheres immersed for 90 min.

**Table 3.** The table shows the concentration used for the Beer–Lambert calibration with subsequent registered absorbance.

| Absorbance (a.u.) | Concentration (M) |
|---|---|
| 0.183 | $1.05 \times 10^{-5}$ |
| 0.331 | $1.58 \times 10^{-5}$ |
| 0.453 | $2.11 \times 10^{-5}$ |
| 0.576 | $2.64 \times 10^{-5}$ |
| 0.706 | $3.16 \times 10^{-5}$ |



**Figure 6.** Linear fitting of absorbance against the five known concentrations. Slope of the line represents the Beer–Lambert coefficient of absorption.
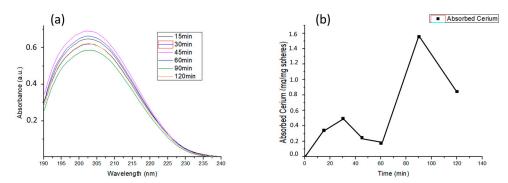


**Figure 7.** The figures show the behaviour of the Ce solution with spheres at different times. (**a**) Shows the UV spectra for the different immersion times; (**b**) shows instead the average absorption of molecules for each time.

*3.2. Coating Characterization*

Two different coatings were prepared (Table 2):

1. One with 1 layer of coating with spheres (Ti1DS).
2. One with 1 layer of coating with spheres and 1 layer without spheres (Ti1DS1DT).
3. The characterization of the coatings is reported below.

### 3.2.1. Surface Morphology

A microstructural characterization of the coatings was performed using SEM. A representative SEM image of the surface of Ti1DS samples is shown in Figure 8. The surface of the coatings appeared uniform, but some cracks and detached particles were detected. The presence of the particles could be attributed to the presence of bigger PVA particles. The particles could induce surface stresses, which could result in the cracking of the deposited coating. A similar type of morphology was already reported in the literature [7], and a coating thickness of about 500 nm was reported in that case following the same sol–gel dip coating procedure [7].
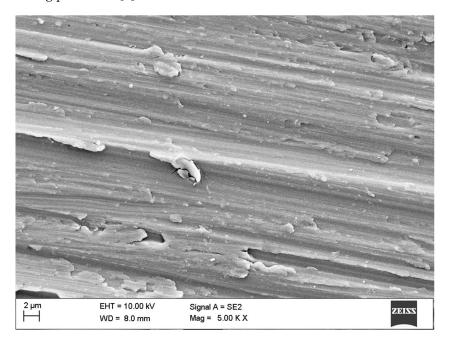


**Figure 8.** SEM micrographs of Ti1DS sample's surface.

Figure 9 shows the surface morphology of sample Ti1DS1DT. From the pictures it can be seen that the surface of the sample was homogeneous. The coating seemed to be more compact and with fewer defects than the Ti1DS samples (Figure 8). This type of appearance is similar to what previous findings on titania coatings without spheres found [9].
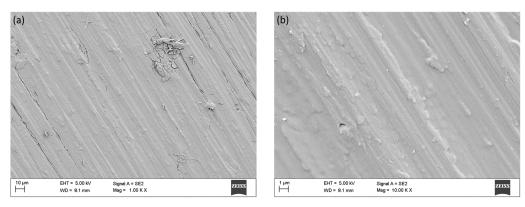


**Figure 9.** SEM micrograph of the surface of Ti1DS1DT at 1 kx (**a**) and 10 kx (**b**).

Chemical composition by XPS (Table 4) reveals a ratio between O1s and Ti2P signals very close to 2:1 confirming the formation of $TiO_2$. The presence of N1s associated with the nitrate group was also detected (1%at) while no signal of Ce was observed. The absence of Ce signal could be linked to the strong interaction between Ce ions and PVA hydroxyl groups [43,44]. In detail, when samples are heat-treated, the polymer with Ce ions strongly

bounded may soften and distribute uniformly throughout the coating. Such occurrence may lead the Ce concentration under the XPS detectable limit.

**Table 4.** The table shows the results of XPS analysis.

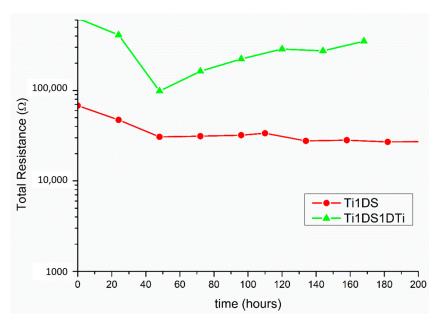| Name | Peak BE (eV) | FWHM (eV) | Atomic (%) | Chemical State |
|---|---|---|---|---|
| Al2p | 72.9 | 0.5 | 0.4 | metal |
| C1s A | 282.4 | 2.2 | 1.2 | carbide |
| C1s B | 284.9 | 2.2 | 21.5 | aliphatic |
| C1s C | 287.3 | 2.2 | 3.4 | carboxyl |
| N1s A | 397.7 | 2.9 | 1.0 | nitride |
| N1s B | 400.6 | 2.9 | 1.2 | C–N |
| N1s C | 405.4 | 2.9 | 0.4 | nitrate |
| O1s A | 531.1 | 1.6 | 31.1 | oxides |
| O1s B | 532.6 | 1.6 | 9.0 | $OH^-$ |
| O1s C | 534.2 | 1.6 | 3.3 | O=C |
| Ti2p3 A | 455.9 | 2.2 | 7.4 | $Ti_2O_3$ |
| Ti2p3 B | 457.9 | 2.2 | 6.3 | $TiO_{2-x}$ |
| Ti2p3 C | 459.5 | 2.2 | 6.9 | $TiO_2$ |

### 3.2.2. EIS Analysis of Coatings

The corrosion resistance of the samples was then evaluated using EIS. The total resistance of the system has been reported in Figure 10 for both Ti1DS and Ti1DS1DT. The samples Ti1DS and Ti1DS1DT showed a similar behaviour for the first 48 h of immersion, when the total resistance decreased, but after 48 h of immersion the behaviour started to increase. This effect was more evident for the system Ti1DS1DT, where after the initial decrease the resistance increased until it approached the starting value, about 200 kΩ. The increase was less evident for the samples Ti1DS. In this case, the total resistance decreased after 48 h from about 67 kΩ to about 30 kΩ. The corrosion resistance of the sample remained stable for the whole immersion time, 206 h. This kind of behaviour is different from previous research on hybrid titania coatings [9] and could be due to the presence of Ce-loaded spheres. In fact, the cerium nitrate loaded in the spheres could deposit on the corroded surface and protect the coating [20,35]. In Figure 10, an initial decrease with time can also be noted (up to 48 h exposure time for Ti1DS1DT). This could be due to the fact that the outer spheres could dissolve when in contact with the water, leading to an increase in the porosity, with a consequent decrease in the resistance of the total resistance. While the reaction progresses, there is an increase in alkalinity that causes the precipitation of Ce as Ce hydroxide, hence the increase in resistance.
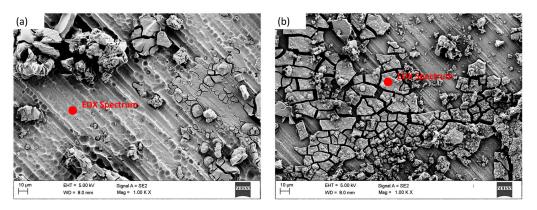
### 3.2.3. Morphology Analysis after Corrosion

After exposure, the samples were analysed using SEM/EDS. All the samples were coated in gold, and this is reflected in the presence of gold in the spectra. The result of the analysis for Ti1DS is shown in Figures 11 and 12. As it can be seen from the figures, the surface shows damage on the coating, which exposes the substrate's surface, inducing corrosion. Part of the coating seems to have remained on the surface. This could explain the lower resistance recorded for Ti1DS (Figure 10). Figure 12 shows the EDS spectrum taken on the surface, showing the presence of Al and Cl only, confirming the exposure of the substrate to the environment. The presence of the coating on the surface (Ti and O) can also be seen. It is worth noting that the Ce peak was not detected on the surface of the metal. This could be due to the fact that the amount of Ce in the coating was below the detection limit of the EDX.

**Figure 10.** Temporal behaviour of the total resistance of Ti1DS (red) and Ti1DS1DT (green). The total resistance is presented in logarithmic scale.



**Figure 11.** SEM micrographs of Ti1DS after corrosion test at 1 kx at different locations (**a**,**b**). EDS of the red points are shown in Figure 12.
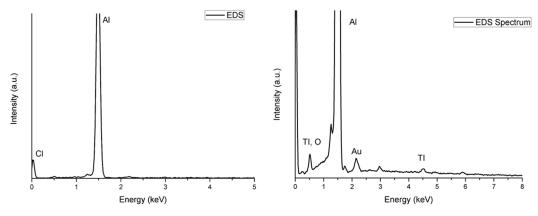


**Figure 12.** EDS spectra of sample Ti1DS after exposure from the pictures in Figure 11.

The SEM micrographs for the sample Ti1DS1DT are shown in Figure 13. From the micrographs it can be seen how the surface of the sample looks mainly undamaged by corrosion, with no exposure of the substrate. The employment of cerium-nitrate-loaded PVA spheres was seen to be effective for corrosion protection; Ce has been seen to be effective as an inhibitor [24,45]. Part of the surface shows some cracks. This would explain

the difference in resistance observed between the two samples (see Figure 10), with the sample Ti1DS1DT showing higher total resistance with respect to the Ti1DS sample. The difference could be due to the absence of spheres in the outer layer. This layer could be able to close the cracks present on the surface before exposure. The EDS spectrum showed in Figure 14 confirms the presence of the coating on the surface.
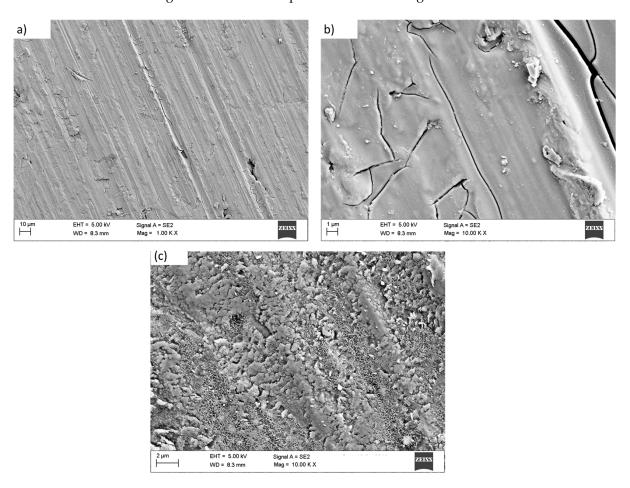


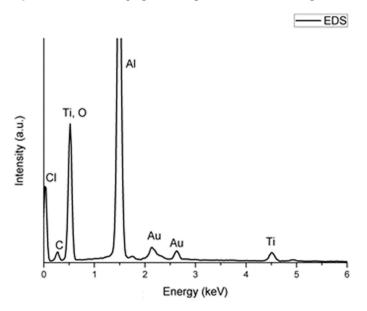**Figure 13.** SEM micrograph of sample Ti1DS1DT after exposure at 1 kx (**a**), 5 kx (**b**), and 10 kx (**c**).



**Figure 14.** EDS spectrum of Ti1DS1DT sample.

### 3.2.4. Electrochemical Analysis after Surface Scratch

A further set of samples was prepared to assess the self-healing ability of the coating. This was performed by introducing a defect (scratch) on the surface of the samples with a blade (Figure 15).
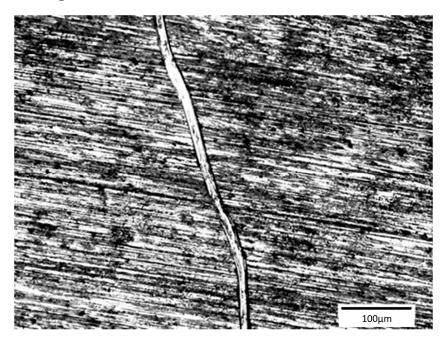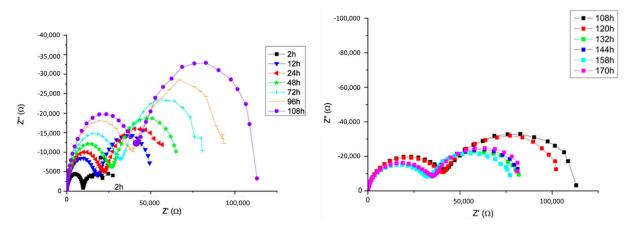


**Figure 15.** Optical microscopy of the scratch made on the samples' surfaces (Ti1DS).

Figure 16 shows a selection of Nyquist plots obtained for the scratched Ti1DS sample. The spectra were collected during the entire exposure time, at different time intervals, with the first set of spectra taken every 6 h, and then every 12 h or 24 h. From the graphs an increase in resistance with increasing exposure time can be observed. This behaviour is the opposite to what is observed in Figure 10 and by Mori et al. [9] in samples not containing spheres. The initial resistance of the scratched sample was around 30 kΩ after 2 h of immersion and then it started to increase with time, almost doubling after 24 h of immersion. After 108 h of exposure the resistance of the sample increased, approaching values around 100 kΩ. After 108 h of immersion the resistance of the sample started to decrease until it reached 75 kΩ after 170 h of exposure.
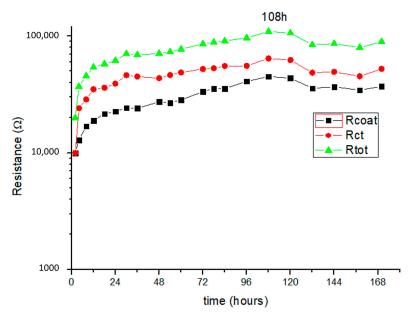


**Figure 16.** A selection of Nyquist plots of Ti1DS up to 108 h (left-hand side) and from 108 h to 170 h (right-hand side) exposure in 3% NaCl solution.

Nyquist plots were then analysed using the equivalent circuit reported in Figure 3. The temporal behaviour for the various resistances has been extracted (Figure 17). The
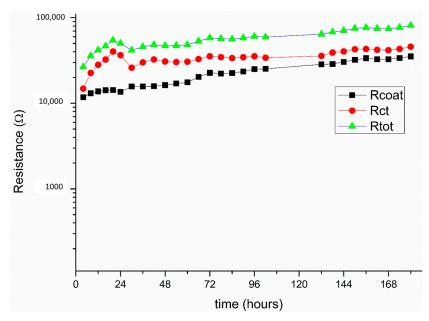
figure shows the total resistance (the green curve), the charge transfer contribution (red), and the coating resistance (black). From Figure 17 the increase in the total resistance of the system was due to the simultaneous increase in both contributions, the charge transfer and coating.



**Figure 17.** Time behaviour of the resistance of the sample Ti1DS. The resistance is presented on a logarithmic scale.

Figure 18 shows the temporal behaviour of the resistances for Ti1DS1DT. The resistance of the system started to increase a few hours after the immersion. From the graphs, it can also be seen that the increase in the total resistance of the system was due to the coating and charge transfer contribution, as in the previous sample (Figure 17).



**Figure 18.** Time behaviour for the resistance of the system Ti1DS1DT. The resistance is presented on a logarithmic scale.
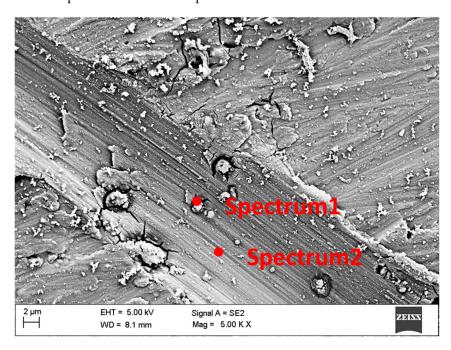
The behaviour observed for those two samples could be explained with the presence of spheres and an inhibitor (cerium nitrate). The Ce could deposit as Ce-oxide around the corrosion areas [20,36]. The samples of Ti1DS1DT did not show a decrease in corrosion

resistance after 108 h of exposure, as shown by the sample Ti1DS (Figures 16 and 17). This could be due to the presence of the second layer, which could fill the cracks shown in the first layer of coating. This is also reflected by the magnitude of the resistance that is constantly more than 1 order of magnitude higher than the sample Ti1DS (see Figures 17 and 18).

### 3.2.5. SEM Analysis after Surface Scratch

After exposure, the surfaces of the samples were analysed using SEM/EDS. Figure 19 shows the scratch on the surface of Ti1DS after exposure. The surface of the sample seems to be still coated, in contrast to what was observed with the sample without scratch. EDS spectra were also collected in the locations shown in Figure 19. The resulting spectra are shown in Figure 20. Figure 20 shows that the coating is not present inside the cracked area, while the presence of corrosion products is shown.



**Figure 19.** SEM micrograph of Ti1DS with scratch after corrosion test at 5 kx, with location of EDS spectra.
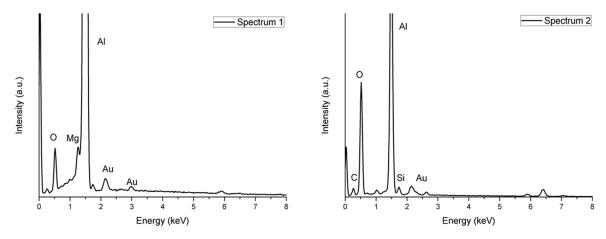


**Figure 20.** EDS spectra for the sample Ti1DS with scratch, from locations shown in Figure 19.

Figure 21 shows the SEM micrograph of Ti1DS1DT after exposure, and the location of the scratch. From the image, it can be seen how the morphology differs from the Ti1DS sample (Figure 19). Cracks on the coating are visible in this case, and this could be due

to the presence of a layer of coating without spheres, which could be damaged by both scratch and corrosion.
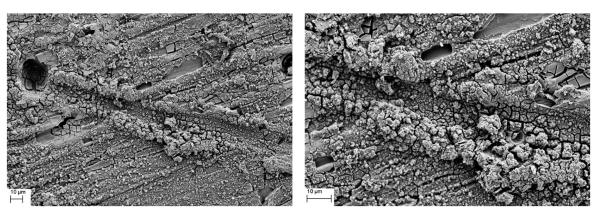


**Figure 21.** SEM micrograph of Ti1DS1DT sample with scratch after exposure.

## 4. Conclusions

Self-healing $TiO_2$-based coatings for corrosion protection of Al alloys were prepared via the sol–gel method. The coating was composed of a $TiO_2$-based matrix and PVA (poly(vinyl-alcohol)) microspheres filled with cerium nitrate. The loaded spheres were added to provide the self-healing ability. Two different coatings were prepared, one made of one layer of coating with spheres, and the second one made of one layer of coating with spheres and a second layer of coating without spheres.

The SEM (scanning electron microscopy) analysis of the sample Ti1DS1DT showed a more compact and less defected (cracks) coating than the Ti1DS sample. This could result in a better corrosion resistance. The higher corrosion resistance was confirmed by the EIS (electro-chemical impedance spectroscopy) analysis. The EIS showed how the Ti1DS1DT had a higher resistance with respect to the Ti1DS samples. Ti1DS1DT sample also showed an increase in total corrosion resistance with the exposure time in the NaCl solution. This behaviour could be due to the presence of the inhibitor, which could have been released by the spheres in contact with the water solution and then deposited on the surface as a protective layer.

To prove the self-healing ability, a defect (scratch) was introduced in a second set of samples. The EIS analysis showed how both coatings shown increased their total corrosion resistance, charge transfer resistance, and coating resistance, with increasing exposure time. The resistance of the scratched samples reached the same values shown by the sample with no induced defect. The sample with 1 layer of coating (Ti1DS) showed an initial increase in total resistance, which was then followed by a decrease after 108 h of exposure. The same behaviour was not observed for the coating made of two layers (Ti1DS1DT). The presence of the second layer could improve the lifetime of the coatings, covering the cracks left on the first layer of coating.

**Author Contributions:** S.M. contributed with the data curation, collection and analysis; S.M. drafted the paper and edited. G.M. was involved in the Conceptualization, project administration, funding and supervision; F.R.L. was involved in the methodology, data analysis and supervision. All authors have read and agreed to the published version of the manuscript.

**Institutional Review Board Statement:** Not applicable.

**Informed Consent Statement:** Not applicable.

**Data Availability Statement:** The data that support the findings of this study are available from the corresponding author, [S.M.], upon reasonable request.

## References

1. Park, R.M.; Bena, J.F.; Stayner, L.T.; Smith, R.J.; Gibb, H.J.; Lees, P.S.J. Hexavalent chromium and lung cancer in the chromate industry: A quantitative risk assessment. *Risk Anal.* **2004**, *24*, 1099–1108. [CrossRef] [PubMed]
2. Pan, L.; He, L.; Niu, Z.; Xiao, P.; Zhou, W.; Li, Y. Corrosion behavior of ytterbium hafnate exposed to water-vapor with $Al(OH)_3$ impurities. *J. Eur. Ceram. Soc.* **2023**, *43*, 612–620. [CrossRef]
3. He, L.; Pan, L.; Zhou, W.; Niu, Z.; Chen, X.; Chen, M.; Zhang, Q.; Pan, W.; Xiao, P.; Li, Y. Thermal corrosion behavior of $Yb_4Hf_3O_{12}$ ceramics exposed to calcium-ferrum-alumina-silicate (CFAS) at 1400 °C. *J. Eur. Ceram. Soc.* **2023**, *43*, 4114–4123. [CrossRef]
4. Kok, W.H.; Sun, X.; Shi, L.; Wong, K.C.; Mitchell, K.A.R.; Foster, T. Formation of zinc phosphate coatings on AA6061 aluminum alloy. *J. Mater. Sci.* **2001**, *36*, 3941–3946. [CrossRef]
5. Dabalà, M.; Ramous, E.; Magrini, M. Corrosion resistance of cerium-based chemical conversion coatings on AA5083 aluminium alloy. *Mater. Corros.* **2004**, *55*, 381–386. [CrossRef]
6. Parsa, M.; Hosseini, S.M.A.; Jamalizadeh, E.; Saheb, V. Preparation and corrosion protective properties of titania-containing modified self-assembled nanophase particle (TMSNAP) sol–gel on AA2024 aluminum alloy. *Mater. Corros.* **2013**, *64*, 821–830. [CrossRef]
7. Liu, T.; Zhang, F.; Xue, C.; Li, L.; Yin, Y. Structure stability and corrosion resistance of nano-$TiO_2$ coatings on aluminum in seawater by a vacuum dip-coating method. *Surf. Coat. Technol.* **2010**, *205*, 2335–2339. [CrossRef]
8. Jothi, K.J.; Palanivelu, K. Praseodymium oxide modified hybrid silane coatings for anti-corrosion applications. *Surf. Eng.* **2016**, *32*, 47–52. [CrossRef]
9. Mori, S.; Lamastra, F.R.; Kaciulis, S.; Soltani, P.; Montesperelli, G. Low-temperature titania coatings for aluminium corrosion protection. *Corros. Eng. Sci. Technol.* **2018**, *53*, 44–53. [CrossRef]
10. G-Berasategui, E.; Bayón, R.; Zubizarreta, C.; Barriga, J.; Barros, R.; Martins, R.; Fortunato, E. Corrosion resistance analysis of aluminium-doped zinc oxide layers deposited by pulsed magnetron sputtering. *Thin Solid Films* **2015**, *594*, 256–260. [CrossRef]
11. Sivapragash, M.; Kumaradhas, P.; Retnam, B.S.J.; Joseph, X.F.; Pillai, U.T.S. Taguchi based genetic approach for optimizing the PVD process parameter for coating ZrN on AZ91D magnesium alloy. *Mater. Des.* **2016**, *90*, 713–722. [CrossRef]
12. Lugscheider, E.; Krämer, G.; Barimani, C.; Zimmermann, H. PVD coatings on aluminium substrates. *Surf. Coat. Technol.* **1995**, *74*, 497–502. [CrossRef]
13. Ramesh, C.S.; Sekhar, N.; Keshavamurthy, R.; Pramod, S. A study on slurry erosion and corrosion behaviour of HVOF sprayed titania coatings. *Int. J. Surf. Sci. Eng.* **2015**, *9*, 55–68. [CrossRef]
14. Thim, G.P.; Oliveira, M.A.S.; Oliveira, E.D.A.; Melo, F.C.L. Sol–gel silica film preparation from aqueous solutions for corrosion protection. *J. Non-Cryst. Solids* **2000**, *273*, 124–128. [CrossRef]
15. Yang, X.F.; Tallman, D.E.; Gelling, V.J.; Bierwagen, G.P.; Kasten, L.S.; Berg, J. Use of a sol--gel conversion coating for aluminum corrosion protection. *Surf. Coat. Technol.* **2001**, *140*, 44–50. [CrossRef]
16. Wang, T.; Du, J.; Ye, S.; Tan, L.; Fu, J. Triple-Stimuli-Responsive Smart Nanocontainers Enhanced Self-Healing Anticorrosion Coatings for Protection of Aluminum Alloy. *ACS Appl. Mater. Interfaces* **2019**, *11*, 4425–4438. [CrossRef]
17. Manasa, S.; Jyothirmayi, A.; Siva, T.; Sathiyanarayanan, S.; Gobi, K.V.; Subasri, R. Effect of inhibitor loading into nanocontainer additives of self-healing corrosion protection coatings on aluminum alloy A356.0. *J. Alloys Compd.* **2017**, *726*, 969–977. [CrossRef]
18. Castro, Y.; Özmen, E.; Durán, A. Integrated self-healing coating system for outstanding corrosion protection of AA2024. *Surf. Coat. Technol.* **2020**, *387*, 125521. [CrossRef]
19. Grigoriev, D.; Shchukina, E.; Shchukin, D.G. Nanocontainers for Self-Healing Coatings. *Adv. Mater. Interfaces* **2017**, *4*, 1600318. [CrossRef]
20. Pepe, A.; Aparicio, M.; Duran, A.; Cere, S. Cerium hybrid silica coatings on stainless steel AISI 304 substrate. *J. Sol-Gel Sci. Technol.* **2006**, *39*, 131–138. [CrossRef]
21. Lamaka, S.V.; Montemor, M.F.; Galio, A.F.; Zheludkevich, M.L.; Trindade, C.; Dick, L.F.; Ferreira, M. Novel hybrid sol–gel coatings for corrosion protection of AZ31B magnesium alloy. *Electrochim. Acta* **2008**, *53*, 4773–4783. [CrossRef]
22. Lee, A.-C.; Lin, R.-H.; Yang, C.-Y.; Lin, M.-H.; Wang, W.-Y. Preparations and characterization of novel photocatalysts with mesoporous titanium dioxide ($TiO_2$) via a sol–gel method. *Mater. Chem. Phys.* **2008**, *109*, 275–280. [CrossRef]
23. Znaidi, L. Sol-gel-deposited ZnO thin films: A review. *Mater. Sci. Eng. B Solid State Mater. Adv. Technol.* **2010**, *174*, 18–30. [CrossRef]
24. Gong, Y.; Geng, J.; Huang, J.; Chen, Z.; Wang, M.; Chen, D.; Wang, H. Self-healing performance and corrosion resistance of novel $CeO_2$-sealed MAO film on aluminum alloy. *Surf. Coat. Technol.* **2021**, *417*, 127208. [CrossRef]
25. Cacciotti, I.; Nanni, F.; Campaniello, V.; Lamastra, F.R. Development of a transparent hydrorepellent modified $SiO_2$ coatings for glazed sanitarywares. *Mater. Chem. Phys.* **2014**, *146*, 240–252. [CrossRef]
26. Bagalà, P.; Lamastra, F.R.; Kaciulis, S.; Mezzi, A.; Montesperelli, G. Ceria/stannate multilayer coatings on AZ91D Mg alloy. *Surf. Coat. Technol.* **2012**, *206*, 4855–4863. [CrossRef]

27. Simonsen, M.E.; Søgaard, E.G. Sol-gel reactions of titanium alkoxides and water: Influence of pH and alkoxy group on cluster formation and properties of the resulting products. *J. Sol-Gel Sci. Technol.* **2010**, *53*, 485–497. [CrossRef]

28. McDonagh, C.; Sheridan, F.; Butler, T.; MacCraith, B.D. Characterisation of sol-gel-derived silica films. *J. Non-Cryst. Solids* **1996**, *194*, 72–77. [CrossRef]

29. Wang, D.; Bierwagen, G.P. Sol–gel coatings on metals for corrosion protection. *Prog. Org. Coat.* **2009**, *64*, 327–338. [CrossRef]

30. Mudali, U.K.; Sridhar, T.M.; Rajendran, N. Electrophoretic deposition of $TiO_2$ and $TiO_2$+ $CeO_2$ coatings on type 304L stainless steel. *Surf. Eng.* **2013**, *23*, 267–272. [CrossRef]

31. Shanaghi, A.; Chu, P.K.; Moradi, H. Effect of Inhibitor Agents Addition on Corrosion Resistance Performance of Titania Sol--Gel Coatings Applied on 304 Stainless Steel. *Surf. Rev. Lett.* **2016**, *24*, 1750055. [CrossRef]

32. Poznyak, S.K.; Zheludkevich, M.L.; Raps, D.; Gammel, F.; Yasakau, K.A.; Ferreira, M.G.S. Preparation and corrosion protective properties of nanostructured titania-containing hybrid sol–gel coatings on AA2024. *Prog. Org. Coat.* **2008**, *62*, 226–235. [CrossRef]

33. Zand, R.Z.; Verbeken, K.; Adriaens, A. Electrochemical assessment of the self-healing properties of cerium doped sol-gel coatings on 304L stainless steel substrates. *Int. J. Electrochem. Sci.* **2012**, *7*, 9592–9608. [CrossRef]

34. Du, J.; Wang, Z.; Wei, Z.; Yao, J.; Song, H. An environmental friendly self-healing coating with Silane/Ce-ZSM-5 zeolite structure for corrosion protection of aluminum alloy. *Surf. Coat. Technol.* **2022**, *436*, 128290. [CrossRef]

35. Pepe, A.; Aparicio, M.; Cere, S.; Duran, A. Preparation and characterization of cerium doped silica sol–gel coatings on glass and aluminum substrates. *J. Non Cryst. Solids* **2004**, *348*, 162–171. [CrossRef]

36. Schem, M.; Schmidt, T.; Gerwann, J.; Wittmar, M.; Veith, M.; Thompson, G.E.; Molchan, I.; Hashimoto, T.; Skeldon, P.; Phani, A.; et al. $CeO_2$-filled sol--gel coatings for corrosion protection of AA2024-T3 aluminium alloy. *Corros. Sci.* **2009**, *51*, 2304–2315. [CrossRef]

37. Montemor, M.F.; Pinto, R.; Ferreira, M.G.S. Chemical composition and corrosion protection of silane films modified with $CeO_2$ nanoparticles. *Electrochim. Acta* **2009**, *54*, 5179–5189. [CrossRef]

38. Yabuki, A.; Yamagami, H.; Noishiki, K. Barrier and self-healing abilities of corrosion protective polymer coatings and metal powders for aluminum alloys. *Mater. Corros.* **2007**, *58*, 497–501. [CrossRef]

39. Lamaka, S.V.; Zheludkevich, M.L.; Yasakau, K.A.; Serra, R.; Poznyak, S.K.; Ferreira, M.G.S. Nanoporous titania interlayer as reservoir of corrosion inhibitors for coatings with self-healing ability. *Prog. Org. Coat.* **2007**, *58*, 127–135. [CrossRef]

40. Nesterova, T.; Dam-Johansen, K.; Pedersen, L.T.; Kiil, S. Microcapsule-based self-healing anticorrosive coatings: Capsule size, coating formulation, and exposure testing. *Prog. Org. Coat.* **2012**, *75*, 309–318. [CrossRef]

41. Nesterova, T. *Self-Healing Anticorrosive Coatings*; Technical University of Denmark: Kongens Lyngby, Denmark, 2012.

42. Schneider, C.A.; Rasband, W.S.; Eliceiri, K.W. NIH Image to ImageJ: 25 years of image analysis. *Nat. Methods* **2012**, *9*, 671–675. [CrossRef] [PubMed]

43. Abdelaziz, M. Cerium (III) doping effects on optical and thermal properties of PVA films. *Phys. B Condens. Matter* **2011**, *406*, 1300–1307. [CrossRef]

44. Ali, F.M.; Kershi, R.M.; Sayed, M.A.; AbouDeif, Y.M. Evaluation of structural and optical properties of Ce3+ ions doped (PVA/PVP) composite films for new organic semiconductors. *Phys. B Condens. Matter* **2018**, *538*, 160–166. [CrossRef]

45. Ren, S.; Meng, F.; Li, X.; Cui, Y.; Liu, R.; Liu, Y.; Hu, X.; Liu, L.; Wang, F. A self-healing epoxy composite coating based on pH-responsive PCN-222 smart containers for long-term anticorrosion of aluminum alloy. *Corros. Sci.* **2023**, *221*, 111318. [CrossRef]